An integrative proteotranscriptomics approach reveals new ADAM9 substrates and downstream pathways

Congyu Lu[1,2‡], Xiaolu Xu[1‡], Neha Sindhu[1,2‡], Jessica Rainey[1], Shawn W. Polson[2,3], Jing Qiu[2,4] and Shuo Wei[1,2*]

[1] Department of Biological Sciences, University of Delaware, Newark, DE 19716, USA

[2] Center for Bioinformatics and Computational Biology, University of Delaware, Newark, DE 19713, USA

[3] Department of Computer and Information Sciences, University of Delaware, Newark, DE 19716, USA

[4] Department of Applied Economics and Statistics, University of Delaware, Newark, DE 19716, USA

[‡] These authors contributed equally to this work.

[*] Correspondence: swei@udel.edu

Running title: Identifying ADAM9 substrates and targets

Keywords: Ectodomain shedding; ADAM9; proteotranscriptomics; FOXO

Abstract

Membrane protein shedding is a key regulatory mechanism for cell signaling and adhesion, and dysregulated shedding is associated with diseases. Many membrane proteases can catalyze shedding, but the substrate spectra and downstream targets of these “sheddases” remain largely elusive. While secretomics-based methods have been applied to the systematic identification of sheddase substrates, these methods are not always effective and do not provide much information on downstream targets. Here we developed an integrative proteotranscriptomics approach to uncover the transcriptional and post-transcriptional targets of the disintegrin metalloproteinase ADAM9, a sheddase that has been implicated in solid tumors, autoimmunity, inflammatory diseases and COVID-19. This systematic approach revealed signaling pathways downstream of ADAM9, including the oncogenic mTOR and tumor suppressor FOXO pathways. We further identified several direct and indirect substrates for ADAM9, which may mediate the pathophysiological roles of ADAM9 in various diseases. Of note, some of these substrates are difficult to detect by secretomics. This new approach can be applied to other sheddases to systematically identify their substrates and targets.

Introduction

Ectodomain shedding refers to the proteolysis of membrane proteins that releases the entire or part of the ectodomain. Shedding is a key regulatory mechanism for cellular processes such as signaling and adhesion. Over 70 proteases can catalyze shedding, including a dozen members of the disintegrin metalloproteinase (ADAM) family, which function as canonical sheddases [1]. Abnormal shedding can contribute to disease pathology. For example, elevated levels of ADAM9, the sheddase that is the focus of this study, have been implicated in several diseases, such as solid tumors, autoimmune diseases, chronic obstructive pulmonary disease (COPD) and COVID-19, whereas loss of ADAM9 leads to retinal degeneration [2-6]. However, despite the importance of ADAM9 and many other sheddases, their substrates and other targets remain largely elusive [1, 7]. This information is not only needed for understanding the mechanisms of action for these sheddases, but also for assessing the adverse effects when targeting them for therapeutic purposes.

Currently, proteomics is essentially the only method for systematic identification of sheddase substrates. Most of the published proteomics studies focused on the secretome, as the shed ectodomains of substrates can often be detected in the conditioned media of cultured cells or tissue, and their abundance is altered when sheddase activity is manipulated [8]. These secretomics-based methods have identified numerous substrates for the “housekeeping” sheddases such as ADAM10 and 17 [1], but are not effective for certain other sheddases with fewer substrates, such as ADAM15 [9, 10]. A possible explanation for false negative results of these methods is that the shed ectodomain of

some substrates may remain attached to the membrane or are quickly turned over, and are hence not present in significant amount in the secretome. One example is the Notch receptors, which are associated with Notch ligands after cleavage by ADAM10, until being internalized and degraded [11]. False positive is another problem, as many differentially expressed proteins (DEPs) in the secretome may be regulated through other mechanisms such as transcription, but cannot be distinguished from *bona fide* shedding substrates by secretomics alone. Finally, secretomics provides little information on downstream genes and pathways, which are also important for mediating sheddase function. Therefore, it is necessary to develop complementary methods to systematically identify sheddase substrates and targets.

This study aimed to establish a new integrative proteotranscriptomics approach to identify sheddase substrates and targets, by using ADAM9 as an example. We carried out RNA-sequencing and quantitative proteomics for HCT116 colon cancer cells with and without ADAM9 knockdown (KD; Fig. 1A). The two omics datasets were integrated using two-way Orthogonal Partial Least Squares (O2PLS) analyses to identify transcriptionally and post-transcriptionally regulated protein targets of ADAM9. Among the post-transcriptional targets that negatively correlate with ADAM9, cell-surface proteins were selected as candidate substrates (Fig. 1B). Using this approach, we have successfully uncovered two downstream signaling pathways and three substrates for ADAM9, which may contribute to the pathological roles of this versatile sheddase.

Results

Characterizing and integrating the transcriptome and cellular proteome regulated by ADAM9 in HCT116 cells

HCT116 cells were chosen for this study due to their stable diploid karyotype that is suitable for omics analyses [12]. We recently showed that ADAM9 cleaves ephrin-B1 and -B2 to promote downstream Akt kinase activity in HCT116 and SW620 colorectal cancer (CRC) cells [13]. To systematically identify other ADAM9 substrates and targets, we knocked down ADAM9 in HCT116 cells using the well characterized siRNA AD9-1 [13]. RNA-seq and multiplexed quantitative proteomics with tandem mass tag (TMT) labeling were performed for control and ADAM9 KD cells. Principle component analyses for both omics data show clear segregation of ADAM9 KD samples from the controls (Fig. S1 and S2). Volcano plots of differentially regulated genes (DEGs) and DEPs (FDR<0.05) are shown in Fig. 1C and D, and heat maps of the top DEGs and DEPs in Fig. 1E and F. The transcriptome and proteome data were integrated using the R package OmicsPLS to identify the transcriptional and post-transcriptional targets as described in Fig. 1B and Methods. Transcriptional and post-transcriptional targets that positively and negatively correlated with ADAM9 (FC>1.2 for DEP) are listed in Table S1 and S2, respectively.

mTOR and FOXO are signaling pathways downstream of ADAM9 in HCT116 cells

To search for major signaling pathways downstream of ADAM9, we carried out KEGG pathway enrichment analysis for the DEGs (FC>1.5), as altered cell signaling often leads to large changes in transcriptome. Among the top 10 pathways (Fig. 2A), mTOR and FOXO are two major pathways downstream of Akt [14]. A comparison of our DEGs

(FC>1.5, q<0.05) with those obtained previously using the mTOR inhibitor Torin-1 [15] shows significant overlap (p=1.5E-04; Fig. 2B and Table S3). The validation of mTOR signaling as a target pathway of ADAM9 in HCT116 cells has been published elsewhere [13]. Akt also downregulates FOXO signaling by phosphorylating FOXO transcription factors to facilitate their nuclear export and degradation [16]. Interestingly, FOXO3, the only FOXO family member detected in HCT116 cells, was one of the top post-transcriptionally upregulated proteins upon ADAM9 KD (FC=1.74, q=2.8E-06). There is also a significant overlap between our DEGs and the genes previously found to be FOXO3 targets [17](p=0.006; Fig. 2C and Table S4). We confirmed the upregulation of FOXO3 with western blotting using both AD9-1 and a second siRNA targeting ADAM9 (AD9-2; Fig. 2D and S3); no significant alteration of the *FOXO3* mRNA was found (Fig. 2E). Three FOXO3 target genes (*MUC13*, *THBS1*, and *GDA*) were selected from Table S4, and their upregulation upon ADAM9 KD was validated using RT-qPCR (Fig. 2E). Consistent with these findings, KD of ADAM9 leads to increased levels of nuclear FOXO3, as shown by immunocytochemistry (ICC; Fig. 2F). Together, these data indicate that ADAM9 suppresses FOXO signaling in HCT116 cells.

Identifying candidate substrates for ADAM9 from post-transcriptional targets

Upon ADAM9 KD, substrates are expected to accumulate on the membrane unless there are additional feedbacks to regulate their protein levels. Among the post-transcriptional targets that negatively correlate with ADAM9 (FC>1.2 for DEP), 188 were annotated as membrane proteins in UniProt. Further analysis showed that 64 of these membrane proteins are localized on the cell surface and hence may serve as potential substrates for

ADAM9. These include 35 single-pass transmembrane (29 type I, 3 type II, 1 type IV and 2 unknown), 26 multi-pass transmembrane, and 2 glycosylphosphatidylinositol-anchored proteins (Table S5).

ALCAM, IL10RB and IGSF8 are ADAM9 substrates with possible disease relevance

We next selected several of the candidate substrates for validation. These included ALCAM, IGSF8, and IL10RB. KD of ADAM9 downregulated the shed ALCAM and IGSF8 in the conditioned media and concomitantly upregulated the full-length proteins in the cell lysates (Fig. 3A, E). Conversely, overexpression of wild-type ADAM9, but not the protease-dead E348A mutant, enhanced shed ALCAM levels in the conditioned media (Fig. 3B), suggesting that ADAM9 protease activity is required for ALCAM shedding. Since ALCAM is known as a substrate for ADAM17 [18], we further examined if ADAM9 regulates ALCAM shedding indirectly via ADAM17 by using HCT116 cells with ADAM17 knocked out (Fig. 3C). In the absence of ADAM17, ectopic wild-type ADAM9 but not the E348A mutant still decreased the full-length ALCAM in the cell lysates and increased the shed ectodomain in the conditioned media (Fig. 3D), suggesting that ADAM9-mediated shedding of ALCAM is independent of ADAM17. In contrast, both wild-type ADAM9 and the E/A mutant increased shed IGSF8 and decreased the full-length protein (Fig. 3F). Thus, IGSF8 is likely an indirect substrate for ADAM9. Although we were unable to detect the shed IL10RB in the conditioned media, the full-length protein was upregulated upon ADAM9 KD (Fig. 3G). Interestingly, the shed IL10RB ectodomain was found in the cell lysates when wild-type ADAM9, but not

the E/A mutant, was overexpressed (Fig. 3H). Since IL10RB primarily exists in complex with other receptor subunits such as IL10RA [19, 20], this indicates that IL10RB ectodomain shed by ADAM9 remains associated with these proteins on the membrane. Thus, we were able to identify ADAM9 substrates that are not released into the conditioned media and hence could not be identified by secretomics approaches.

Discussion

To date, only a handful of substrates have been reported for ADAM9, all of which were identified through candidate but not systematic approaches [7]. Here we developed a new high-throughput and nonbiased approach to systematically screen for ADAM9 substrates. Among the validated substrates identified in this study, ALCAM and IGSF8 play important roles in solid tumor progression, and elevated ALCAM shedding in CRC samples correlates with poor patient survival [21-23]. IL10RB is upregulated in both COPD and COVID-19 patients and is one of the top risk factors for severe COVID-19; it is also a potential therapeutic target for autoimmune diseases such as inflammatory bowel disease, which can lead to CRC [24-26]. We further show that ADAM9 promotes mTOR signaling, an oncogenic pathway [27], while suppressing FOXO signaling, a tumor suppressor pathway [28], providing an explanation for the involvement of this sheddase in multiple types of solid tumors. These findings will shed new light on the pathophysiology of ADAM9-related diseases.

Secretomics and transcriptomics have been used as individual approaches to identify sheddase substrates and transcriptional targets, respectively; to our knowledge the

integration of two or more omics approaches has not been explored for shedding. Here, we demonstrate the power of combining proteomics and transcriptomics to identify sheddase substrates and targets. Using ADAM9 as an example, we show that this method can differentiate between transcriptional and post-transcriptional targets, and reveal substrates that are not detectable by secretomics (such as IL10RB). Our future efforts will be focused on comparing and combining these results with those obtained from secretomics. The integration of multiple omics methods will greatly improve the coverage and accuracy of sheddase substrate and target identification.

Methods

Plasmids and reagents

The expression constructs encoding wild-type and protease-dead E348A mutant ADAM9 were generated in our previous study [13]. The cDNA construct for mouse ALCAM was purchased from Dharmacon (Clone ID: 3501215). The cDNA sequence encoding mouse ALCAM$^{28\text{-}583}$ was subcloned into a pCS2+ expression vector containing a signal peptide followed by an in-frame FLAG tag using the BspEI and XbaI restriction sites (Fig. S4). Sequences of all PCR primers used in this study are shown in Table S6. The siRNAs used in this study include control siRNA (SIC) (Cell Signaling Technology (CST) 6568), ADAM9 siRNA-1 (AD9-1) (CST 11968), and ADAM9 siRNA-2 (AD9-2) (Ambion 4390826). Antibodies used in this study include rabbit anti-ADAM9 (CST 4151, 1:1,000), mouse anti-ALCAM (Santa Cruz 74558, 1:200), mouse anti-IL10RB (R&D Systems MAB874, 5 μg/ml), rabbit anti-FOXO3 (CST 2497, 1:1,000 for western blotting, and 1:100 For immunocytochemistry), rabbit anti-IGSF8 (Sigma 011917,

1:500), HRP-conjugated rabbit anti-mouse (CST 7076, 1:2,000), HRP-conjugated goat anti-rabbit (CST 7074; 1:2,000), HRP-conjugated mouse anti-β-actin antibody (CST 12262, 1:2,000), and Alexa Fluor™ 594-conjugated goat anti-rabbit antibody (Thermal fisher A-11012, 1:1,000 for ICC).

Cell culture and transfection

Parental HCT116 were purchased from ATCC (CCL-247), and HCT116 cells with ADAM17 knocked out were from Abcam (ab266873). These cells were cultured in McCoy's 5A medium (ATCC) containing 10% fetal bovine serum (FBS) and 1% Pen-Strep (100 U/mL penicillin and 100 μg/mL streptomycin) in 5% CO_2 at 37°C. Cells were grown to 60% confluence and transfected with siRNA using lipofectamine RNAiMAX transfection reagent (Invitrogen). The medium was refreshed 12 h after transfection, and the cells were further incubated for another 48 h. For secretomics analysis and cleavage assays, cells were washed with phosphate buffered saline (PBS) and changed to serum-free medium 12 h after the transfection, and the cells were further incubated in serum free medium for another 48 h.

RNA-seq Analysis

Total RNA was extracted from the cells using RNeasy Mini Kit (QIAGEN, USA) according to the manufacturer's instructions. The quality of the RNA was estimated using the A260:A280 ratio, and RNA degradation and contamination were monitored by electrophoresis in 1% agarose gels. The integrity and size distribution of RNA were evaluated using a Bioanalyzer. The total RNA samples were treated with DNase I to

eliminate DNA contamination. Illumina RNA-Seq library construction and sequencing were conducted by the University of Delaware DNA Sequencing & Genotyping Center (RRID:SCR_012230, Newark, DE). Six replicates of each treatment were used for the RNA-seq (paried end with 101 read length) performed with the Illumina HiSeq 2500 system (Illumina).

After obtaining the RNA-Seq raw data in FASTQ format, the quality of the raw data was evaluated with FastQC (0.11.5) (Babraham Institute Bioinformatics, Cambridge, UK), a quality control tool for high throughput sequence data. The low-quality read ends and adapter sequences were removed, and the low-quality reads were filtered out using Trim Galore (0.4.4) (Babraham Institute Bioinformatics, Cambridge, UK). After the trimming and filtering, all the reads were aligned to the hg19 human reference genome using TopHat2 (2.1.1). HTseq (0.11) was used to count how many reads map to each annotated gene. The differential gene expression analysis was conducted using the R package edgeR (3.20.9), which provide statistical routines for determining differential expression based on a negative binomial model. False discovery rate (FDR) was used for multiple test correction, and the exact test in edgeR was conducted to determine the differentially expressed genes (DEGs) with a cutoff threshold of FDR < 0.05 and fold change > 1.5. Pathway enrichment analysis of the DEGs was performed using Enrichr.

Cellular Proteomics Analysis

Proteins were reduced, alkylated, and purified by chloroform/methanol extraction prior to digestion with sequencing grade modified porcine trypsin (Promega). Tryptic peptides

were labeled using tandem mass tag isobaric labeling reagents (Thermo) following the manufacturer's instructions and combined into one 10-plex sample group. The labeled peptide multiplex was separated into 46 fractions on a 100 x 1.0 mm Acquity BEH C18 column (Waters) using an UltiMate 3000 UHPLC system (Thermo) with a 50 min gradient from 99:1 to 60:40 buffer A: B ratio under basic pH conditions, and then consolidated into 18 super-fractions. Each super-fraction was then further separated by reverse phase XSelect CSH C18 2.5 um resin (Waters) on an in-line 150 x 0.075 mm column using an UltiMate 3000 RSLCnano system (Thermo). Peptides were eluted using a 60 min gradient from 98:2 to 60:40 buffer A: B ratio. Eluted peptides were ionized by electrospray (2.2 kV) followed by mass spectrometric analysis on an Orbitrap Eclipse Tribrid mass spectrometer (Thermo) using multi-notch MS3 parameters. MS data were acquired using the FTMS analyzer in top-speed profile mode at a resolution of 120,000 over a range of 375 to 1500 m/z. Following CID activation with normalized collision energy of 35.0, MS/MS data were acquired using the ion trap analyzer in centroid mode and normal mass range. Using synchronous precursor selection, up to 10 MS/MS precursors were selected for HCD activation with normalized collision energy of 65.0, followed by the acquisition of MS3 reporter ion data using the FTMS analyzer in profile mode at a resolution of 50,000 over a range of 100-500 m/z. Buffer A = 0.1% formic acid, 0.5% acetonitrile, Buffer B = 0.1% formic acid, 99.9% acetonitrile. Both buffers were adjusted to pH 10 with ammonium hydroxide for offline separation.

Proteins were identified and MS3 reporter ions were quantified using MaxQuant (Max Planck Institute) against the UniprotKB *Homo sapiens* database (January 2021) with a

parent ion tolerance of 3 ppm, a fragment ion tolerance of 0.5 Da, and a reporter ion tolerance of 0.003 Da. Scaffold Q+S (Proteome Software) was used to verify MS/MS-based peptide and protein identifications (protein identifications were accepted if they could be established with less than 1.0% false discovery and contained at least two identified peptides; protein probabilities were assigned by the Protein Prophet algorithm) and to perform reporter ion-based statistical analysis [29]. Protein TMT MS3 reporter ion intensity values were analyzed using the ProteiNorm app, a user-friendly tool for normalization, imputation of missing values, and differential expression analysis [30]. The Linear Models for Microarray Data (limma) with empirical Bayes (eBayes) smoothing to the standard errors were used to conduct the differential expression analysis [31]. Proteins with an FDR < 0.05 and a fold change > 1.2 were considered to be differentially expressed proteins.

Integration of transcriptome and proteome data to identify ADAM9 substrates and targets

The transcriptome and cellular proteome were integrated using the OmicsPLS R package (PMID: 30309317). OmicsPLS is the implementation of O2PLS, which is a symmetrical multivariate regression method that integrates two datasets [32, 33]. It decomposes the variation in two data matrices into three parts: the joint component shared by two datasets, the orthogonal components specific for each dataset, and residual error. The join components induce the relationship between the two datasets and can be viewed as the representation of the integration. We define transcriptional targets as DEPs whose mRNA and protein positively correlate with each other, and post-transcriptional targets as DEPs

whose mRNA and protein do not have a significant positive correlation (Fig. 1B). Pre-processed data was fitted to the O2PLS model to obtain the systematic and non-systematic components of the data, with the former including the joint component, and dataset-specific 'orthogonal' component. For both types of targets, we further determined whether they were positively or negatively correlated with ADAM9. To do this, we tested for a significant positive or negative correlation of the systematic variation of the protein with that of ADAM9 in the proteome. Potential substrates of ADAM9 cleavage are cell-surface proteins that are post-transcriptional targets negatively correlated with ADAM9. Cell Surface proteins were determined from their annotation as per UniProt (Release 2024_03) subcellular localization. The surface proteins were further prioritized based on their types.

Western Blotting and RT-qPCR

Cells were lysed in the cell lysis buffer (Cell Signaling) and the concentration of the protein was determined using the Bicinchoninic acid (BCA) assay (Thermo Scientific) with bovine serum albumin (BSA) as standard. For the western blotting, the same amount of protein was loaded on SDS-PAGE gels and then electrotransferred onto PVDF membranes (Bio-Rad). After blocking for 1 hour with 5% BSA and incubating for 1 hour with primary antibody, signals were detected by peroxidase-conjugated secondary antibodies using chemiluminescence reaction (Bio-Rad). β-actin was used as the loading control.

Total RNA was reverse transcribed into cDNA using the iScript cDNA Synthesis Kit (Bio-Rad Laboratories) with DNase I treatment (Qiagen). RT-qPCR was performed using the qMAX Green Low Rox qPCR Mix (Accuris) according to the manufacturer's instructions. All samples were assayed in triplicate, and data were analyzed using the Comparative CT Method with GAPDH as the reference gene. The RT-qPCR primers are shown in Table S6.

Immunocytochemistry

HCT116 cells were grown to 60% confluence on Poly-L-lysine coated coverslips (Neuvitro) and transfected with siRNA using lipofectamine RNAiMAX transfection reagent (Invitrogen). The medium was refreshed 12 h after transfection, and the cells were further incubated for another 48□h. Cells were then fixed in PBS containing 4% paraformaldehyde for 10 min and permeabilized by incubation in PBS containing 0.2% Triton X-100 for 10 min at room temperature. After washing in PBS three times for 5 min, cells were blocked with 1% BSA for 30 min. Cells were then incubated with FOXO3 antibody (1:100) overnight at 4□, washed in PBS three times for 5 min, and incubated with anti-rabbit secondary antibody (1:1000) for 1 h at room temperature. After washing in PBS three times for 5 min, coverslips were incubated in DAPI (1:10,000) for 1 min at room temperature. Imaging was performed with confocal microscopy LSM 880, AxioObserver, and objective Plan-Apochromat 20x. Nuclear regions were first defined by DAPI stain and the red signal intensities within the nuclear regions were measured.

Data availability

Data supporting the findings of this work are available within the paper and its Extended View figures and tables files. RNA-seq data and proteomics data will be deposited to public repositories upon publication.

Acknowledgements

This work was supported by the US National Institute of Health (R01 GM114105, P20 GM104316, U54 GM104941 and R24GM137786 to S.W.). JR was supported by an NIH training grant (T32GM133395).

Figure legends

Figure 1. The transcriptome and cellular proteome of HCT116 cells with and without ADAM9 KD. (**A**) Flow chart of our transcriptome and cellular proteome analyses. (**B**) Integration of transcriptome and cellular proteome to identify transcriptional and post-transcriptional targets as well as candidate substrates for ADAM9. (**C, D**) Volcano plots of transcriptome (**C**) and cellular proteome (**D**) showing DEGs and DEPs (FDR<0.05). ADAM9 is highlighted as a positive control. (**E, F**) Heat maps showing top DEGs (**E**) and DEPs (**F**).

Figure 2. ADAM9 regulates mTOR and FOXO signaling in HCT116 cells. (**A**) KEGG pathway enrichment analysis of transcriptome data showing top 10 pathways affected by ADAM9 KD. (**B**, **C**) Venn diagrams showing significant overlaps between the DEGs found in our transcriptome data and published transcriptional targets of mTOR (**B**) and FOXO3 (**C**). (**D**) Western blots of FOXO3 in control and ADAM9 KD cells (3 biological replicates each). Statistics is shown on the right with p-value at the top. (**E**) RT-qPCR results of the indicated genes with and without ADAM9 KD (3 biological replicates each). (**F**) ICC of FOXO3 in control and ADAM9 KD cells. Confocal images were processed with ImageJ to measure the intensity of red fluorescence (FOXO3) within the DAPI-stained area (nucleus).

Figure 3. Identification of ALCAM, IGSF8 and IL10RB as new ADAM9 substrates. HCT116 cells were transfected with the indicated siRNA or expression constructs), and western blotting was performed for conditioned media (CM) or cell lysates (CL) using

antibodies specifically recognizing the ectodomain of the indicated proteins. Three biological replicates are shown for KD experiments, with statistics including p-values on the right. Western blots of endogenous ADAM17 in parental and *ADAM17* knockout (KO) cells are shown in **C**, and shedding of FLAG-tagged ALCAM by myc-tagged wild-type (WT) ADAM9 and the E348A mutant in *ADAM17* KO cells in **D**.

References

1. Lichtenthaler, S.F., M.K. Lemberg, and R. Fluhrer, *Proteolytic ectodomain shedding of membrane proteins in mammals-hardware, concepts, and recent developments.* EMBO J, 2018. **37**(15).
2. Carapito, R., et al., *Identification of driver genes for critical forms of COVID-19 in a deeply phenotyped young patient cohort.* Sci Transl Med, 2022. **14**(628): p. eabj7521.
3. Oria, V.O., P. Lopatta, and O. Schilling, *The pleiotropic roles of ADAM9 in the biology of solid tumors.* Cell Mol Life Sci, 2018. **75**(13): p. 2291-2301.
4. Parry, D.A., et al., *Loss of the metalloprotease ADAM9 leads to cone-rod dystrophy in humans and retinal degeneration in mice.* Am J Hum Genet, 2009. **84**(5): p. 683-91.
5. Umeda, M., et al., *ADAM9 enhances Th17 cell differentiation and autoimmunity by activating TGF-β1.* Proc Natl Acad Sci U S A, 2021. **118**(18).
6. Wang, X., et al., *A Disintegrin and A Metalloproteinase-9 (ADAM9): A Novel Proteinase Culprit with Multifarious Contributions to COPD.* Am J Respir Crit Care Med, 2018. **198**(12): p. 1500-18.
7. Chou, C.W., et al., *An Overview of ADAM9: Structure, Activation, and Regulation in Human Diseases.* Int J Mol Sci, 2020. **21**(20).
8. Yang, C.Y., L. Troeberg, and S.D. Scilabra, *Quantitative Mass Spectrometry-Based Secretome Analysis as a Tool to Investigate Metalloprotease and TIMP Activity.* Methods Mol Biol, 2020. **2043**: p. 265-273.
9. Yang, C.Y., et al., *Quantitative Proteomics Reveals That ADAM15 Can Have Proteolytic-Independent Functions in the Steady State.* Membranes (Basel), 2022. **12**(6).
10. Calligaris, M., et al., *Identification of membrane proteins regulated by ADAM15 by SUSPECS proteomics.* Front Mol Biosci, 2023. **10**: p. 1162504.
11. Schnute, B., T. Troost, and T. Klein, *Endocytic Trafficking of the Notch Receptor.* Adv Exp Med Biol, 2018. **1066**: p. 99-122.
12. Venkataramanan, S., et al., *DDX3X and DDX3Y are redundant in protein synthesis.* RNA, 2021. **27**(12): p. 1577-1588.
13. Chandrasekera, P., et al., *Metalloprotease ADAM9 cleaves ephrin-B ligands and differentially regulates Wnt and mTOR signaling downstream of Akt kinase in colorectal cancer cells.* J Biol Chem, 2022. **298**(8): p. 102225.
14. Manning, B.D. and A. Toker, *AKT/PKB Signaling: Navigating the Network.* Cell, 2017. **169**(3): p. 381-405.
15. Park, Y., et al., *mTORC1 Balances Cellular Amino Acid Supply with Demand for Protein Synthesis through Post-transcriptional Control of ATF4.* Cell Rep, 2017. **19**(6): p. 1083-1090.
16. Huang, H. and D.J. Tindall, *Regulation of FOXO protein stability via ubiquitination and proteasome degradation.* Biochim Biophys Acta, 2011. **1813**(11): p. 1961-4.
17. Eijkelenboom, A., et al., *Genome-wide analysis of FOXO3 mediated transcription regulation through RNA polymerase II profiling.* Mol Syst Biol, 2013. **9**: p. 638.

18. Rosso, O., et al., *The ALCAM shedding by the metalloprotease ADAM17/TACE is involved in motility of ovarian carcinoma cells.* Mol Cancer Res, 2007. **5**(12): p. 1246-53.
19. Shouval, D.S., et al., *Interleukin 10 receptor signaling: master regulator of intestinal mucosal homeostasis in mice and humans.* Adv Immunol, 2014. **122**: p. 177-210.
20. Ahn, D. and A. Prince, *Participation of the IL-10RB Related Cytokines, IL-22 and IFN-λ in Defense of the Airway Mucosal Barrier.* Front Cell Infect Microbiol, 2020. **10**: p. 300.
21. Ferragut, F., et al., *ALCAM/CD166: A pleiotropic mediator of cell adhesion, stemness and cancer progression.* Cytokine Growth Factor Rev, 2021. **61**: p. 27-37.
22. Ding, Y., et al., *EWI2 and its relatives in Tetraspanin-enriched membrane domains regulate malignancy.* Oncogene, 2023. **42**(12): p. 861-868.
23. Hansen, A.G., et al., *Elevated ALCAM shedding in colorectal cancer correlates with poor patient outcome.* Cancer Res, 2013. **73**(10): p. 2955-64.
24. Acevedo, N., et al., *Chronic Obstructive Pulmonary Disease Patients Have Increased Levels of Plasma Inflammatory Mediators Reported Upregulated in Severe COVID-19.* Front Immunol, 2021. **12**: p. 678661.
25. Voloudakis, G., et al., *A translational genomics approach identifies IL10RB as the top candidate gene target for COVID-19 susceptibility.* NPJ Genom Med, 2022. **7**(1): p. 52.
26. Griffin, H., et al., *Neutralizing Autoantibodies against Interleukin-10 in Inflammatory Bowel Disease.* N Engl J Med, 2024. **391**(5): p. 434-441.
27. Xie, J., X. Wang, and C.G. Proud, *mTOR inhibitors in cancer therapy.* F1000Res, 2016. **5**.
28. Calissi, G., E.W. Lam, and W. Link, *Therapeutic strategies targeting FOXO transcription factors.* Nat Rev Drug Discov, 2021. **20**(1): p. 21-38.
29. Nesvizhskii, A.I., et al., *A statistical model for identifying proteins by tandem mass spectrometry.* Anal Chem, 2003. **75**(17): p. 4646-58.
30. Graw, S., et al., *proteiNorm - A User-Friendly Tool for Normalization and Analysis of TMT and Label-Free Protein Quantification.* ACS Omega, 2020. **5**(40): p. 25625-25633.
31. Ritchie, M.E., et al., *limma powers differential expression analyses for RNA-sequencing and microarray studies.* Nucleic Acids Res, 2015. **43**(7): p. e47.
32. Bouhaddani, S.E., et al., *Integrating omics datasets with the OmicsPLS package.* BMC Bioinformatics, 2018. **19**(1): p. 371.
33. Bouhaddani, S.E., et al., *Evaluation of O2PLS in Omics data integration.* BMC Bioinformatics, 2016. **17 Suppl 2**(Suppl 2): p. 11.

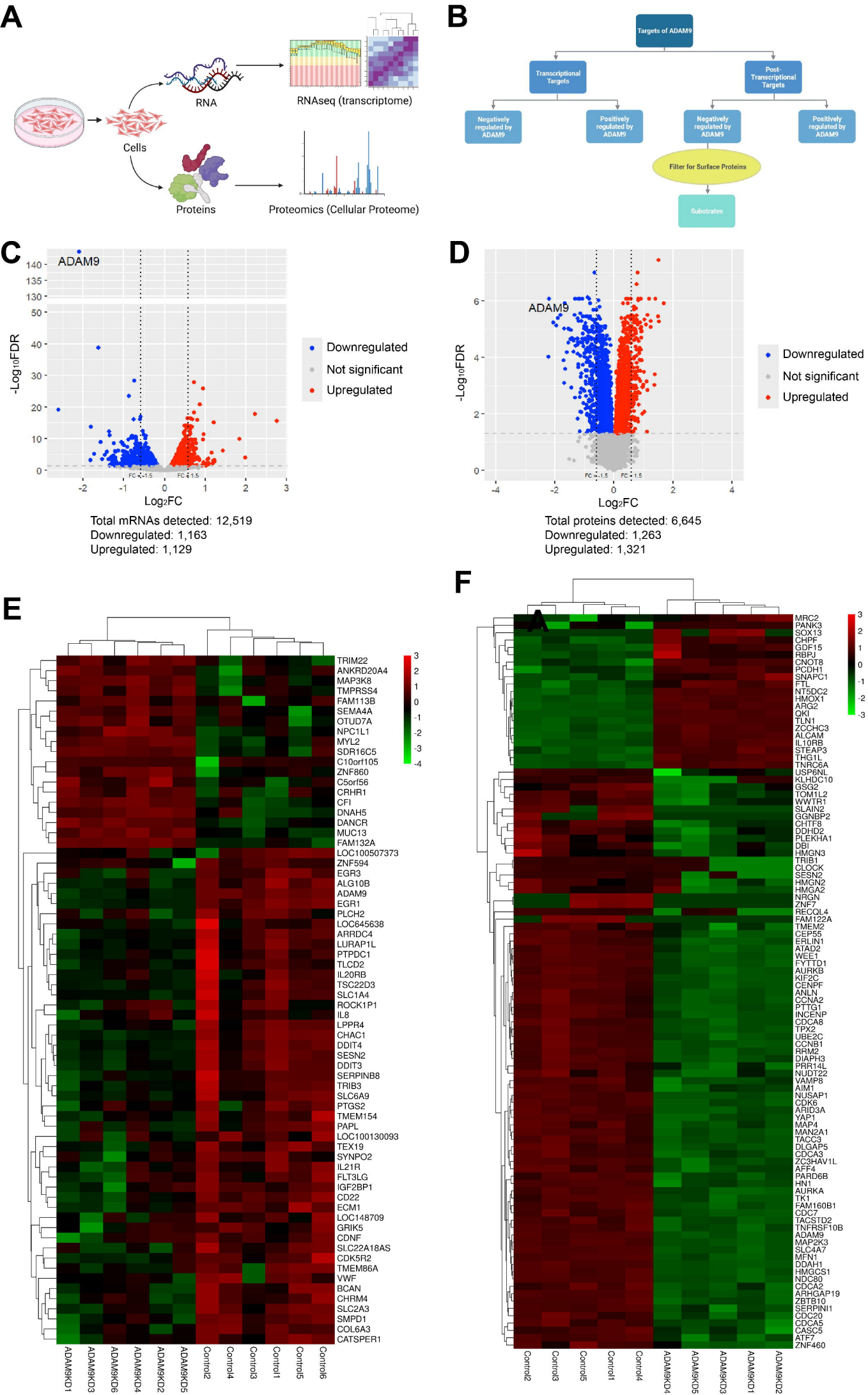
A
RNA
RNAseq (transcriptome)
Cells
Proteins
Proteomics (Cellular Proteome)
B
Targets of ADAM9
Transcriptional Targets
Post-Transcriptional Targets
Negatively regulated by ADAM9
Positively regulated by ADAM9
Negatively regulated by ADAM9
Positively regulated by ADAM9
Filter for Surface Proteins
Substrates
C
ADAM9
-Log10FDR
Log2FC
Downregulated
Not significant
Upregulated
Total mRNAs detected: 12,519
Downregulated: 1,163
Upregulated: 1,129
D
ADAM9
-Log10FDR
Log2FC
Downregulated
Not significant
Upregulated
Total proteins detected: 6,645
Downregulated: 1,263
Upregulated: 1,321
E
TRIM22
ANKRD20A4
MAP3K8
TMPRSS4
FAM113B
SEMA4A
OTUD7A
NPC1L1
MYL2
SDR16C5
C10orf105
ZNF860
C5orf56
CRHR1
CFI
DNAH5
DANCR
MUC13
FAM132A
LOC100507373
ZNF594
EGR3
ALG10B
ADAM9
EGR1
PLCH2
LOC645638
ARRDC4
LURAP1L
PTPDC1
TLCD2
IL20RB
TSC22D3
SLC1A4
ROCK1P1
IL8
LPPR4
CHAC1
DDIT4
SESN2
DDIT3
SERPINB8
TRIB3
SLC6A9
PTGS2
TMEM154
PAPL
LOC100130093
TEX19
SYNPO2
IL21R
FLT3LG
IGF2BP1
CD22
ECM1
LOC148709
GRIK5
CDNF
SLC22A18AS
CDK5R2
TMEM86A
VWF
BCAN
CHRM4
SLC2A3
SMPD1
COL6A3
CATSPER1
ADAM9KD1
ADAM9KD3
ADAM9KD6
ADAM9KD4
ADAM9KD2
ADAM9KD5
Control2
Control4
Control3
Control1
Control5
Control6
F
MRC2
PANK3
SOX13
CHPF
GDF15
RBPJ
CNOT8
PCDH1
SNAPC1
FTL
NT5DC2
HMOX1
ARG2
QKI
TLN1
ZCCHC3
ALCAM
IL10RB
STEAP3
THG1L
TNRC6A
USP6NL
KLHDC10
GSG2
TOM1L2
WWTR1
SLAIN2
GGNBP2
CHTF8
DDHD2
PLEKHA1
DBI
HMGN3
TRIB1
CLOCK
SESN2
HMGN2
HMGA2
NRGN
ZNF7
RECQL4
FAM122A
TMEM2
CEP55
ERLIN1
ATAD2
WEE1
FYTTD1
AURKB
KIF2C
CENPF
ANLN
CCNA2
PTTG1
INCENP
CDCA8
TPX2
UBE2C
CCNB1
RRM2
DIAPH3
PRR14L
NUDT22
VAMP8
AIM1
NUSAP1
CDK6
ARID3A
YAP1
MAP4
MAN2A1
TACC3
DLGAP5
CDCA3
ZC3HAV1L
AFF4
PARD6B
HN1
AURKA
TK1
FAM160B1
CDC7
TACSTD2
TNFRSF10B
ADAM9
MAP2K3
SLC4A7
MFN1
DDAH1
HMGCS1
NDC80
CDCA2
ARHGAP19
ZBTB10
SERPINI1
CDC20
CDCA5
CASC5
ATF7
ZNF460
Control2
Control3
Control5
Control1
Control4
ADAM9KD4
ADAM9KD5
ADAM9KD3
ADAM9KD1
ADAM9KD2

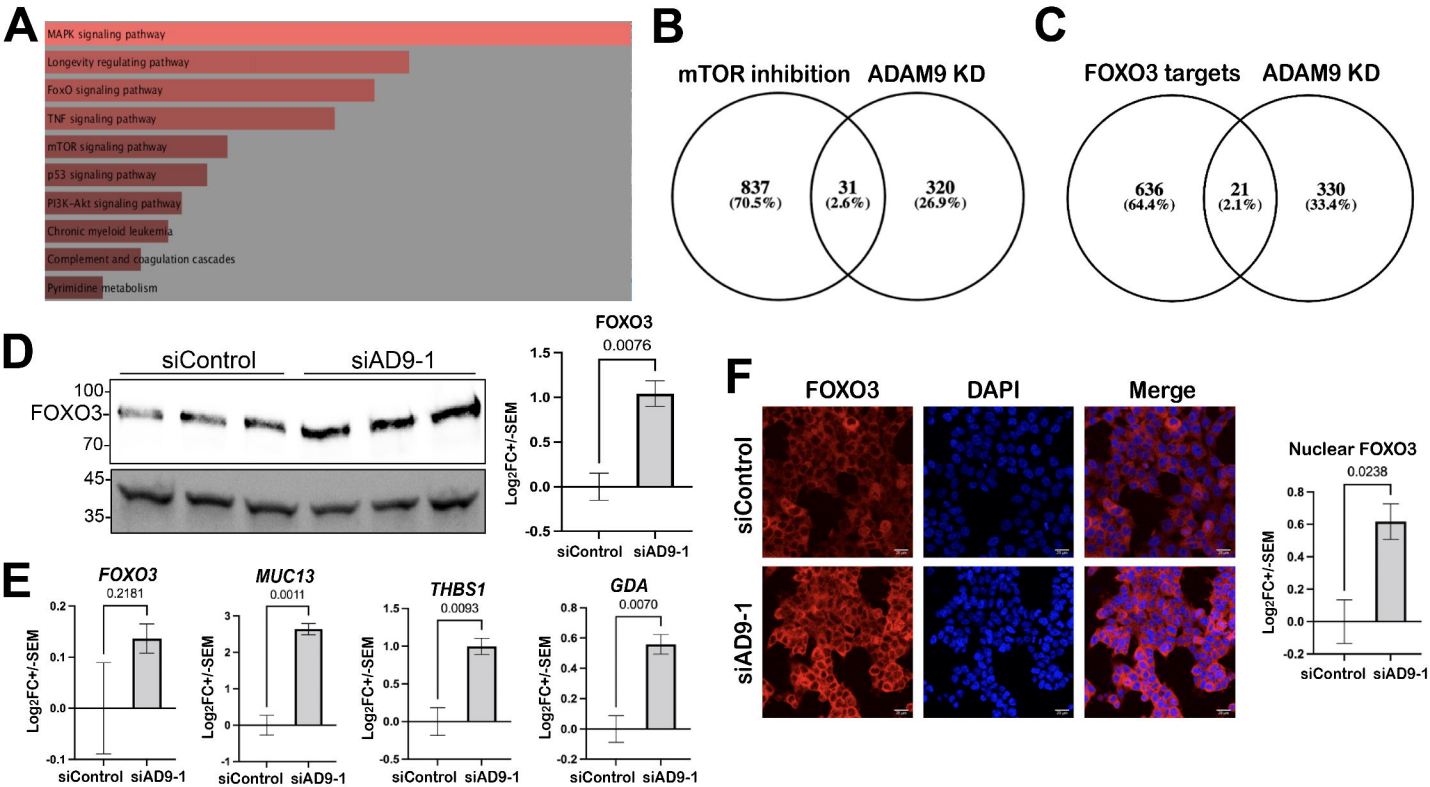
A
MAPK signaling pathway
Longevity regulating pathway
FoxO signaling pathway
TNF signaling pathway
mTOR signaling pathway
p53 signaling pathway
PI3K-Akt signaling pathway
Chronic myeloid leukemia
Complement and coagulation cascades
Pyrimidine metabolism
B
mTOR inhibition
ADAM9 KD
837 (70.5%)
31 (2.6%)
320 (26.9%)
C
FOXO3 targets
ADAM9 KD
636 (64.4%)
21 (2.1%)
330 (33.4%)
D
siControl
siAD9-1
100
FOXO3
70
45
35
FOXO3
0.0076
Log2FC+/-SEM
siControl
siAD9-1
E
FOXO3
0.2181
MUC13
0.0011
THBS1
0.0093
GDA
0.0070
Log2FC+/-SEM
siControl
siAD9-1
F
FOXO3
DAPI
Merge
siControl
siAD9-1
Nuclear FOXO3
0.0238
Log2FC+/-SEM
siControl
siAD9-1

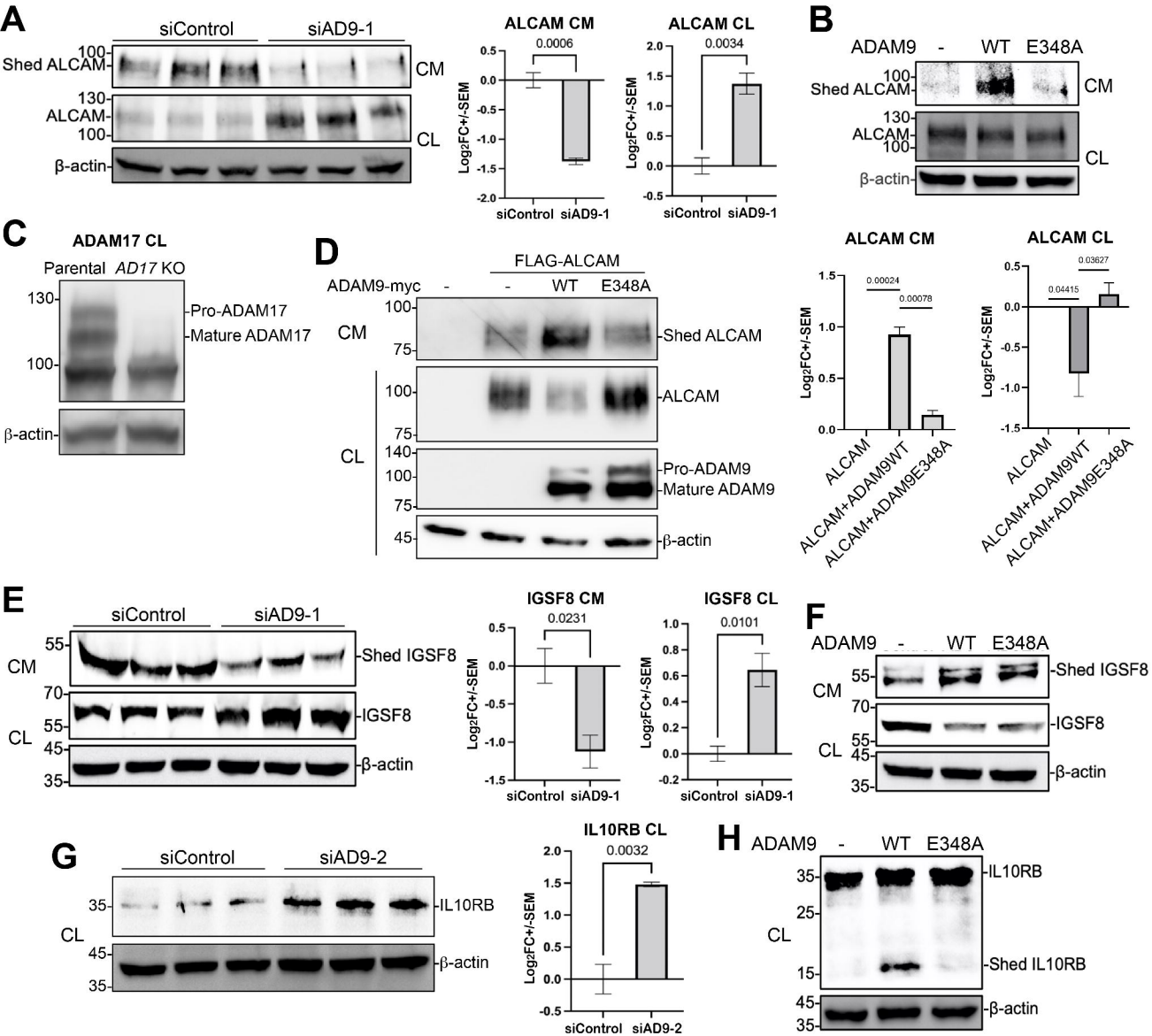
A
siControl
siAD9-1
100
Shed ALCAM
CM
130
ALCAM
100
CL
β-actin
ALCAM CM
0.0006
Log2FC+/-SEM
siControl
siAD9-1
ALCAM CL
0.0034
B
ADAM9
-
WT
E348A
C
ADAM17 CL
Parental
AD17 KO
130
100
Pro-ADAM17
Mature ADAM17
D
FLAG-ALCAM
ADAM9-myc
Shed ALCAM
ALCAM
Pro-ADAM9
Mature ADAM9
0.00024
0.00078
0.04415
0.03627
ALCAM
ALCAM+ADAM9WT
ALCAM+ADAM9E348A
E
IGSF8 CM
0.0231
IGSF8 CL
0.0101
Shed IGSF8
IGSF8
F
G
IL10RB CL
0.0032
IL10RB
H
Shed IL10RB